Medical Engineering and Physics 71 (2019) 79–90

Contents lists available at ScienceDirect

Medical Engineering and Physics

journal homepage: www.elsevier.com/locate/medengphy

Morphologically bioinspired hierarchical nylon 6,6 electrospun assembly recreating the structure and performance of tendons and ligaments

Alberto Sensini[a], Carlo Gotti[a], Juri Belcari[a], Andrea Zucchelli[a], Maria Letizia Focarete[b,c], Chiara Gualandi[b,d], Ivan Todaro[a], Alexander P. Kao[e], Gianluca Tozzi[e], Luca Cristofolini[a,c,*]

[a] Department of Industrial Engineering, Alma Mater Studiorum—University of Bologna, I-40131 Bologna, Italy
[b] Department of Chemistry 'G. Ciamician' and National Consortium of Materials Science and Technology (INSTM, Bologna RU), Alma Mater Studiorum—University of Bologna, I-40126 Bologna, Italy
[c] Health Sciences and Technologies—Interdepartmental Center for Industrial Research (CIRI-HST), Alma Mater Studiorum—University of Bologna, I-40064 Ozzano dell'Emilia, Bologna, Italy
[d] Advanced Mechanics and Materials – Interdepartmental Center for Industrial Research (CIRI-MAM), Alma Mater Studiorum—University of Bologna, I-40123 Bologna, Italy
[e] Zeiss Global Centre, School of Mechanical and Design Engineering, University of Portsmouth, Portsmouth PO1 3DJ, United Kingdom

ARTICLE INFO

Article history:
Received 1 February 2019
Revised 17 May 2019
Accepted 19 June 2019

Keywords:
Bioinspired structures
Electrospinning
Hierarchical devices
Tendons and Ligaments

ABSTRACT

Reconstructions of ruptured tendons and ligaments currently have dissatisfactory failure rate. Failures are mainly due to the mechanical mismatch of commercial implants with respect to the host tissue. In fact, it is crucial to replicate the morphology (hierarchical in nature) and mechanical response (highly-nonlinear) of natural tendons and ligaments. The aim of this study was to develop morphologically bioinspired hierarchical Nylon 6,6 electrospun assemblies recreating the structure and performance of tendons and ligaments. First, we built different electrospun bundles to find the optimal orientation of the nanofibers. A 2nd-level hierarchical assembly was fabricated with a dedicated process that allowed tightly joining the bundles one next to the other with an electrospun sheath, so as to improve the mechanical performance. Finally, a further hierarchical 3rd-level assembly was constructed by grouping several 2nd-level assemblies. The morphology of the different structures was assessed with scanning electron microscopy and high-resolution X-ray tomography, which allowed measuring the directionality of the nanofibers in the bundles and in the sheaths. The mechanical properties of the single bundles and of the 2nd-level assemblies were measured with tensile tests. The single bundles and the hierarchical assemblies showed morphology and directionality of the nanofibers similar to the tendons and ligaments. The strength and stiffness were comparable to that of tendons and ligaments. In conclusion, this work showed an innovative electrospinning production process to build nanofibrous Nylon 6,6 hierarchical assemblies which are suitable as future implantable devices and able to mimic the multiscale morphology and the biomechanical properties of tendons and ligaments.

1. Introduction

The design and development of innovative solutions to repair or substitute injured tendons and ligaments is one of extreme interest in orthopaedic research. In fact, approximately 30 million new cases of tendon and ligament injuries are diagnosed worldwide annually [1]. From over 33 million musculoskeletal injuries per year in the United States alone, almost 50% of them are tendon and ligament related, with about 95,000 new cases annually [2]. The difficulty in healing these tissues is mainly related to their non-linear mechanical properties and complex hierarchical structure, composed of collagen fibers that are axially aligned and organized in different levels of aggregation [3–5]. Above all, due to low cellular activity, the injuries of elderly people generally require the use of permanent inert prosthetic devices [6–8]. An inert polymeric material frequently used for devices in this field is Nylon 6,6, which has been approved as an implantable material [9]. For instance, Nylon 6,6 is found in commercially available suture wires [10,11] and tendon grafts [12].

* Corresponding author at: Department of Industrial Engineering, Alma Mater Studiorum – Università di Bologna, Via Umberto Terracini 28, 40131 Bologna, Italy.
E-mail address: luca.cristofolini@unibo.it (L. Cristofolini).

https://doi.org/10.1016/j.medengphy.2019.06.019
1350-4533/

The most popular examples of inert devices for tendon and ligament are Lars® Ligament, Leeds-Keio® (i.e. Poly-tape®) and Gore-Tex® [12]. In the last two decades, several studies published in literature have assessed the clinical quality of these devices [8]. However, even if they have adequate mechanical behavior, compared to the native tendon or ligament tissue, they have a different morphology and are not hierarchically structured. The Lars® Ligament is composed of aligned microfibers grouped together by an external knitted membrane; Leeds-Keio® (i.e. Poly-tape®) is a totally knitted/waved microfibrous device; while Gore-Tex® is made of groups of aligned microfibers braided together to obtain the final device. However, all these textile patterns produce implantable devices have a very different morphology when compared to a natural tendon or ligament [13]. In fact, tendon or ligament tissue is composed of collagen nanofibers preferentially axially aligned, organized in different levels of aggregation and covered by membranes of randomly arranged collagen nanofibers [3,4,14]. The lack of bioinspired hierarchical organization of these implantable devices, can often cause inflammatory outcomes and post-operative complications [8,12]. Furthermore, several clinical follow-ups of such devices have shown controversial outcomes, in terms of failure or success over a long-term period [8]. Among the others, Lars® Ligament showed the most promising results for long term positive outcomes of the implants and low incidence of revision surgery in Anterior Cruciate Ligament (ACL) applications [15]. However minor episodes of knee stiffness and synovitis were documented in the past [8,15,16]. The published studies about the clinical performances in ACL reconstruction using the Leeds-Keio®, despite several positive results, showed frequent events of re-rupture, tunnel enlargement, synovitis associated with polyester particles, greater pivot-shift and laxity, especially until the early 2000s [17–20]. Moreover different applications of this device were explored to repair other tendons and ligaments such as rotator cuff, knee extensor, Achilles tendon, iliofemoral ligament and ankle lateral ligament [8]. Gore-Tex® devices showed satisfactory results to treat very large rotator cuff tears and patellar reconstructions [21,22], but due to severe osteolytic complications were completely abandoned for ACL applications [8,23,24].

A promising approach to overcome the morphological and mechanical limitations of these devices is offered by the electrospinning technology. Producing polymeric nanofibers by stretching solutions in high electrostatic fields, the electrospinning technique has demonstrated the ability to fabricate scaffolds that mimic the tendon and ligament tissue [25,26]. However, to date no one has used electrospinning to produce complex assemblies that reproduce the hierarchical structure and mechanical properties of a whole tendon or ligament [27].

The aim of this study was to develop morphologically bioinspired hierarchical assemblies (made of inert Nylon 6,6) to replicate the biomechanical response of natural tendons and ligaments. For this reason, three levels of aggregation were investigated: (i) bundles of random and aligned electrospun nanofibers; (ii) a 2nd-level hierarchical assembly built using the most promising type of bundles (aligned nanofibers); (iii) a 3rd-level hierarchical assembly containing several 2nd-levels hierarchical assemblies. For all of these structures, the morphology and the associated mechanical properties were investigated.

2. Materials and methods

In order to develop a complex hierarchical structure, in the first phase two different methods for producing electrospun bundles were developed: in one instance, the nanofibers were randomly aligned, while in the second instance a high alignment of the nanofibers was achieved. The morphology of the bundles was characterized with Scanning Electron Microscopy (SEM) and High-Resolution X-ray Computed Tomography (XCT); mechanical tests were performed to assess the strength and modulus of elasticity of the constructs. The most promising candidates (bundles of aligned nanofibers) were used to produce the 2nd-level hierarchical assemblies, which were again characterized in terms of morphology and mechanical properties. The 3rd-level hierarchical assembly was built by joining three 2nd-level hierarchical assemblies, and its morphology was fully characterized.

2.1. Materials

Nylon 6,6 pellets, kindly provided by DuPont (Wilmington, USA), were dissolved in a trifluoroacetic acid (TFA) (Carlo Erba, Milan, Italy) and acetone (AC) (Sigma Aldrich, Saint-Louis, USA) mixture, in order to obtain the following solution: 15% (w/v) solution of Nylon 6,6 dissolved in TFA:AC = 50:50 (v/v).

2.2. Identification of optimal electrospun bundle preparation

2.2.1. Electrospun bundles production

Electrospun bundles were produced using a laboratory electrospinning machine (Spinbow Lab Unit, Spinbow S.r.1., Bologna, Italy), equipped with a linear sliding spinneret (carrying four syringes ejecting the same polymeric solution) and a rotating drum collector (diameter = 150 mm; length = 500 mm). A syringe pump (KD Scientific 200 series, Illinois, USA) and four glass syringes were used to electrospin the solution. Each syringe was connected to a stainless-steel blunt-ended needle (inner diameter = 0.84 mm) with a PTFE tube. The electrospinning was performed at room temperature (RT) and relative humidity 20–30%. The solution was electrospun with an applied voltage of 20 kV and a feed rate of 0.50 mL h^{-1}. The drum collector was positioned 160 mm away from the needle tips. The sliding spinneret with the four needles had an excursion of 100 mm, with a sliding speed of 1200 mm min^{-1}. The mats of nanofibers were cut circumferentially into strips.

In order to reach the best configuration in terms of fiber orientation and mechanical properties, different electrospun bundles were produced. Bundles made of random fibers were obtained by rotating the drum collector with a low peripheral speed of 0.78 m s^{-1} and for an electrospinning time of 1.5 h (Fig. 1). The mats of random nanofibers were cut into 70 mm wide strips, and manually wrapped to produce bundles, with a cross-sectional diameter of approximately 550–650 micrometers. At the end of the procedure, the bundles (about 470 mm in length) were cut in an extremity and removed from the collector (Fig. 1).

However, in order to improve the mechanical properties of the random bundles (see results section), bundles of aligned nanofibers were produced. To obtain mats of nanofibers preferentially aligned in the direction of drum rotation, the drum collector was rotated with a higher peripheral speed of 22.8 m s^{-1} during an electrospinning time of 3 h. The mats of aligned nanofibers were cut into 50 mm wide strips, and rolled on the drum as previously described.

2.2.2. Morphological investigation of bundles

To examine the surface morphology of the Nylon 6,6 bundles, Scanning Electron Microscopy (SEM) analysis was performed. A commercial SEM (Philips 515 SEM, Amsterdam, Netherlands) was used with a voltage of 15 kV, on samples sputter-coated with gold. The diameter of the nanofibers and their distribution (mean and SD) were measured on the SEM images of 200 fibers, by means of the image analysis software ImageJ [28].

To measure the mean diameter of each bundle a light optical microscope (Axioskop, Zeiss, Pleasanton, CA, USA) equipped with a

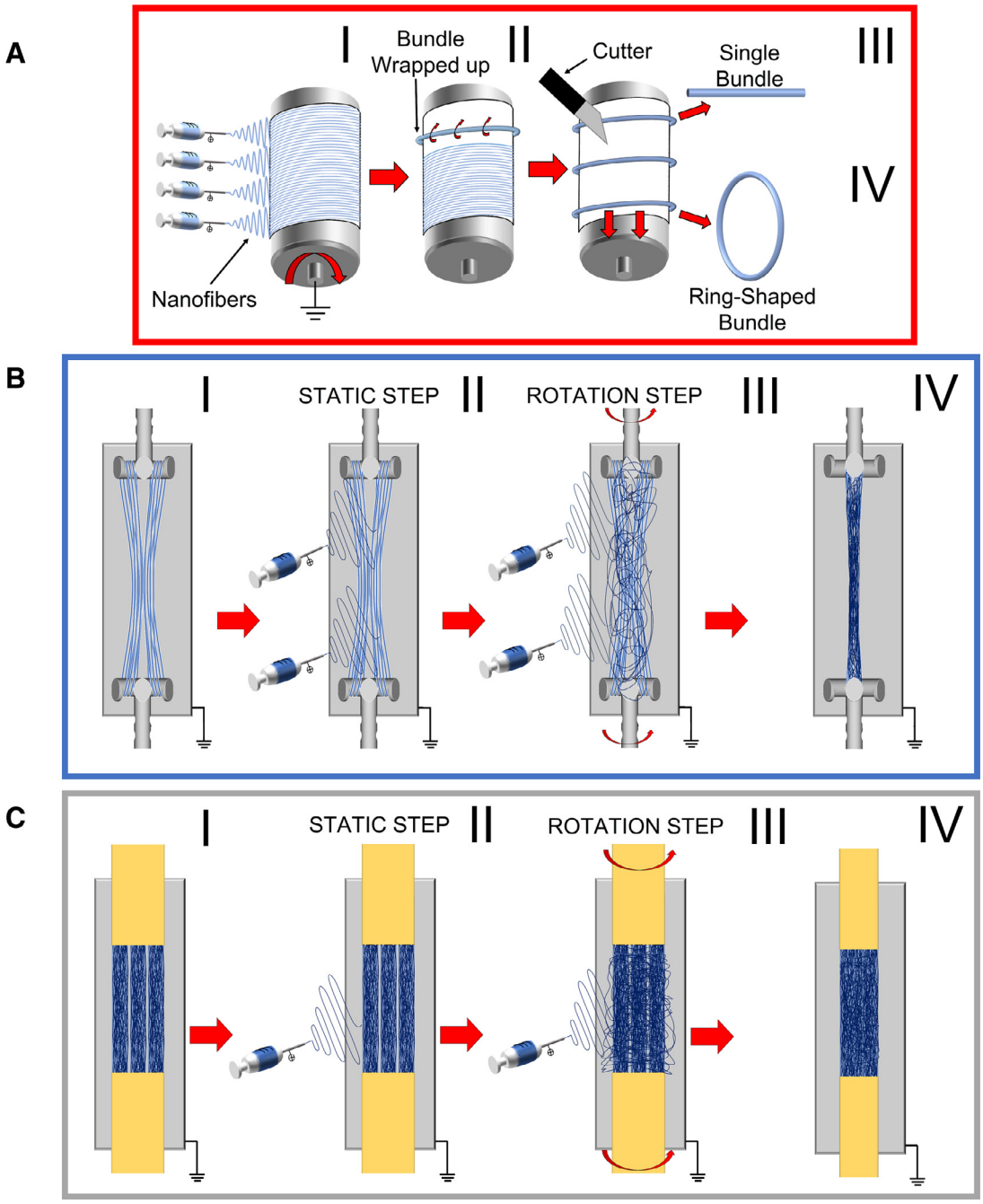

Fig. 1. Electrospinning setups and procedures to produce the bundles and the hierarchical devices. A) Bundles production: I) random or aligned nanofibers were electrospun on the rotating drum collector; II) mats of nanofibers cut in strips and manually wrapped to obtain the bundles; III) Some bundles were cut for remove them from the drum (single bundles); IV) other bundles were removed from the drum without cutting (ring-shaped bundles). B) 2nd-level hierarchical assembly production: I) ring-shaped bundles of aligned nanofiber were hooked on the 6-arms capstan grip; II) electrospun sheath production during the static step; III) during the rotation step the mat of nanofibers was torn from one side of the collector and wrapped around the group of bundles; IV) final 2nd-level hierarchical assembly ready to be tested. B) 3rd-level hierarchical assembly production: I) three 2nd-level hierarchical assembly grouped together; II) electrospun sheath production during the static step; III) during the rotation step the mat of nanofibers was torn from one side of the collector and wrapped around the group of 2nd-level hierarchical assembly; IV) final 3rd-level hierarchical assembly ready to be characterized.

camera (AxioCam MRc, Zeiss, Pleasanton, CA, USA) was used and image analysis was performed using ImageJ [28]. For each bundle, the mean and standard deviation (SD) of ten measurements was computed. To measure the weight of each specimen a precision balance was used (MC 210 P, capacity resolution: 210 g x 0.01 mg, Sartorius, Göttingen, Germany). For each bundle, the mean and SD of three measurements was computed.

In order to investigate the three-dimensional structure of the Nylon 6,6 bundles, high-resolution x-ray tomographic scans were acquired with a laboratory XCT (Versa 510, Zeiss, Pleasanton, CA, USA). For the XCT scans, the following settings were used: 40 kV Voltage, 3 W Power, 75.5 microAmpere tube current. Projections were collected at rotational steps of 0.18° over 360°, with a voxel size 0.4 micrometers, using 14 s exposure time (scanning time of approximately 10 h).

All the XCT images, were reconstructed using the Scout-and-Scan Reconstructor software (Zeiss), and were visualized using XM3DViewer1.2.8 software (Zeiss).

2.2.3. Directionality of the nanofibers in the bundles

In order to quantify the distribution of orientation of the nanofibers in the bundles, the Directionality plugin of ImageJ was used [28–30]. This approach allowed to quantify the amount of nanofibers within a given angle from the axis. The analysis was performed using a Local Gradient Orientation method following a procedure previously validated [31]. For the random nanofiber bundles the Directionality analysis was performed on stacks of five SEM images (magnification = 8000x). For the aligned nanofiber bundle a full volume investigation was performed applying the same procedure to all the slices of the XCT stacks, after reslicing.

2.2.4. Mechanical characterization of the bundles

The mechanical properties of the random and aligned nanofiber bundles were measured with a servo-hydraulic testing machine (8032, Instron, High Wycombe, UK), with $a \pm 1$ kN dynamic cell (Instron, High Wycombe, UK). The force signals had a noise of 0.01 N after filtering. All the specimens were immersed in saline for two minutes before the mechanical test. The test machine was operated in displacement control, adjusting the actuator speed according to the actual specimen length, to obtain a strain rate of 70% s^{-1}. This strain rate is in the range of those experienced by tendons and ligaments during strenuous physiological activities [32–35].

Ten specimens of both random and aligned nanofiber bundles were tested. Dedicated capstan grips (Fig. 5) were used to minimize the stress concentration at the specimens ends. The gauge length was 47.42 mm (this included the free length and the portion of specimen wrapped around the capstans, consistent with the BS EN 12,562:1999 and the ASTM D2256/D2256M-10 (2015) Standards).

The mechanical characterization of the random and aligned bundles was performed to identify the most biomimetic candidate, so just the typical load-strain curves and the force and stress data were analyzed (see Section 2.3.4 and Fig. 2).

2.3. Optimization of the hierarchical assemblies

Based on the most promising configuration from Section 2.2 (see Results), aligned bundles were adopted for the following steps. In order to allow easier handling and stretching of the bundles in the subsequent steps of preparation of the hierarchical structures, the bundles were removed from the collector without any cut, thus obtaining ring-shaped bundles (Fig. 1).

2.3.1. Fabrication of the hierarchical assemblies

In order to reproduce the whole morphology of a tendon or ligament [4,14,27], two different electrospun bioinspired assembly were produced.

To group together different numbers of bundles, an innovative electrospinning procedure to electrospin nanofibrous sheaths was developed (Fig. 1). These sheath were designed to reproduce the morphology of the natural membranes of tendons (endotenon, epitenon) or ligaments (endoligament, epiligament) [4,27]. The same electrospinning parameters previously described were used.

Two custom made stainless-steel 6-arms capstan grips (6 cylindrical arms of 8 mm of diameter each) were fixed in a custom-made rotating electrospinning machine. Then, 24 bundles were hooked on the grips, 4 for each arm (Fig. 1). After this operation, a Nylon 6,6 sheath of nanofibers was electrospun on the group of bundles for 12 h. The custom-made electrospinning apparatus was composed of a high-voltage power supply (FuG Elektronik GmbH, Schechen, Germany), two syringe pumps (KD Scientific Legato 100, Illinois, USA), and two glass syringes containing the polymeric solution, connected to stainless-steel blunt-ended needles (inner diameter = 0.84 mm) by PTFE tubes.

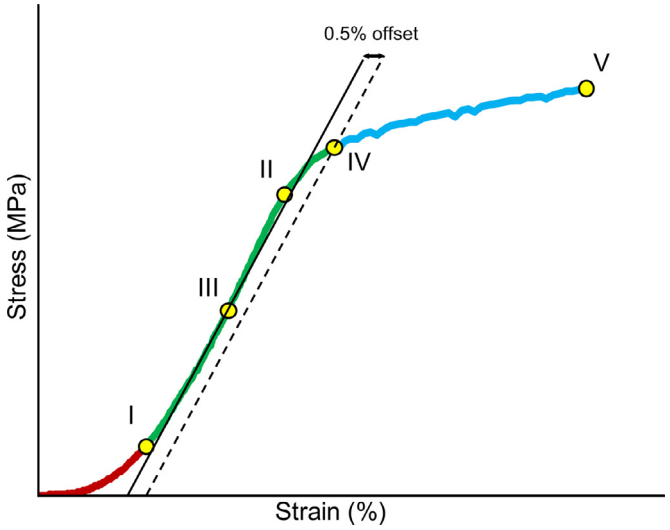

Fig. 2. Post processing of the stress-strain curves. The stress-strain curves were qualitatively similar for the single bundles and for the hierarchical assemblies, but the magnitude of the stress and strain achieved were different. The failure stress (σ_F) (V) was identified as the highest stress in the entire curve. The starting point of the linear region (I) was identified as 20% of the failure stress (σ_F) for the bundles of aligned nanofibers and the 2nd-level hierarchical assembly, and as 5% of the failure stress (σ_F) for the bundles of random nanofibers (the different threshold was required due to the different behaviour of the two types of bundle). The initial toe region (from 0 N to I) was disregarded. An initial guess for the yield strain was visually identified (II). A first linear regression (solid line) was applied to the first 50% of the linear region, between points (I) and (III) (III was half-way between I and II). A second line parallel to the first regression was drawn with an offset of 0.5% strain (dashed line). The limit of proportionality was defined with the 0.5% strain offset criterion as the intersection (IV) between the latter line and the stress-strain curve. The modulus of elasticity (E) was calculated as the slope of a new regression line between (I) and (IV). The unit work to yield (L_Y) and to failure (L_F) were calculated as the integrals under the curves (with the method of trapezoids). Two plots were obtained for each specimen: one reporting the apparent stress, the other one with the net stress.

In order to concentrate the nanofibers on the group of bundles, a flat aluminum collector plate (200 mm high and 50 mm wide) was placed behind the bundles (Fig. 1). To pre-strain the nanofibers of the sheath on the final assembly surface, the group of bundles was in a static position, and intermittently put in rotation (approximately 20 rpm for 1 min every 5 min), while the sheath was being electrospun (Fig. 1).

Finally, in order to produce a hierarchical assembly to completely simulate the structure of a whole tendon or ligament [4,27], including the endotenon/endoligament sheaths and the tertiary fiber bundles inside, a 3rd-level hierarchical assembly was produced. First, three Nylon 6,6 2nd-level hierarchical assemblies, with five ring-shaped bundles each, were produced as previously described (with an electrospinning session of 10 h each). Then, the extremities of the three 2nd-level hierarchical assemblies were tied together with paper tape, and fixed in the machine (Fig. 1). To produce the epitenon/epiligament-like sheath, the same procedure and methods previously described were used, with and electrospinning session of 10 h (Fig. 1).

2.3.2. Morphological investigation of the hierarchical assemblies

The SEM and light optical microscope investigations on the 2nd-level and 3rd-level hierarchical assemblies were performed with the same parameters previously described in Section 2.2.2.

To investigate the three-dimensional structure of the Nylon 6,6 hierarchical assemblies, the XCT scans were acquired with a different high-resolution x-ray tomography system (Versa 520, Zeiss, Pleasanton, CA, USA). The following parameters were used (depending on the shape and thickness of the specimens):

(i) 2nd-level hierarchical assembly: 50 kV Voltage, 4 W Power, 80 microAmpere tube current, 5.27 micrometers voxel size, 1.75 s exposure time, rotational steps of 0.12° over 360°, for a scanning time of 7.5 h; (ii) 3rd-level hierarchical assembly: 50 kV Voltage, 3 W Power, 60 microAmpere tube current, 5.27 micrometers voxel size, 1.75 s exposure time, rotational steps of 0.12° over 360°, for a scanning time of 7.5 h.

All the XCT images, were reconstructed using the Scout-and-Scan Reconstructor software (Zeiss), and were visualized using XM3DViewer1.2.8 software (Zeiss).

2.3.3. Directionality of the nanofibers of the sheath and of the internal bundles

In order to quantify the orientation of the nanofibers in the electrospun sheaths and in the bundles inside the assemblies, the Directionality plugin of ImageJ was used [28–30], as described above in the bundles section. The Directionality analysis was performed with two different approaches derived from Sensini et al. [31].

For the external sheaths, the Directionality analysis was performed on stacks of 5 SEM surface images (magnification = 8000x). To assess the orientation of the bundles inside the hierarchical assemblies, a full volume investigation was performed applying the procedure to all the slices of the XCT stacks, after a reslice.

2.3.4. Mechanical characterization of the hierarchical assemblies

The mechanical characterization was performed both on the ring-shaped bundles and on the 2nd-level hierarchical assemblies (due to limited availability of specimens, the mechanical tests were not performed on the 3rd-level hierarchical assembly).

As the hierarchical assemblies were built with ring-shaped bundles (as opposed to the straight bundles tested before, see 2.2.4) the mechanical test was performed starting from the single ring-shaped bundles. Ten specimens of ring-shaped bundles were tested using capstan grips with the same strain rate as before (Fig. 9). The gauge length was 220 mm (consistent to the ASTM D1414 Standard).

Finally, three specimens of 2nd-level hierarchical assembly were tested. The cross-sectional diameter of each specimen was measured as above (mean and SD between 30 measurements in three different sections). The specimens were weighed with the same precision balance. In order to minimize the stress concentration, the specimens were tested directly on the stainless-steel 6-arms capstan grips, mounted on the Instron testing machine (Fig. 9).

The following indicators were considered: Yield Stress (σ_Y), Yield Strain (ε_Y), Modulus of Elasticity (E), Failure Force (F_F), Failure Stress (σ_F), Failure Strain (ε_F), Unit Work to Yield (L_Y), Unit Work to Failure (L_F) (Fig. 2). The force-displacement curves were converted to stress-strain curves using two different approaches:

- To describe the macroscopic mechanical behavior of the specimen, the apparent stress was computed dividing the force by the cross-sectional area measured before the test.
- To quantify the net mechanical properties, the net stress was also computed dividing the apparent stresses by the volume fraction (v) of the specimens.
- The apparent and the net modulus of elasticity (E), and unit works to failure were computed (L_Y, L_F)

The volume fraction (v) was calculated by using the equation:

$$v = w/(L \cdot A \cdot \rho) \quad (1)$$

Where:

w is the weight of the specimen
L is length of the specimen,
A is the cross-sectional area of the specimen
ρ is the density of the raw material (Nylon 6,6 = 1.14 g/cm^3)

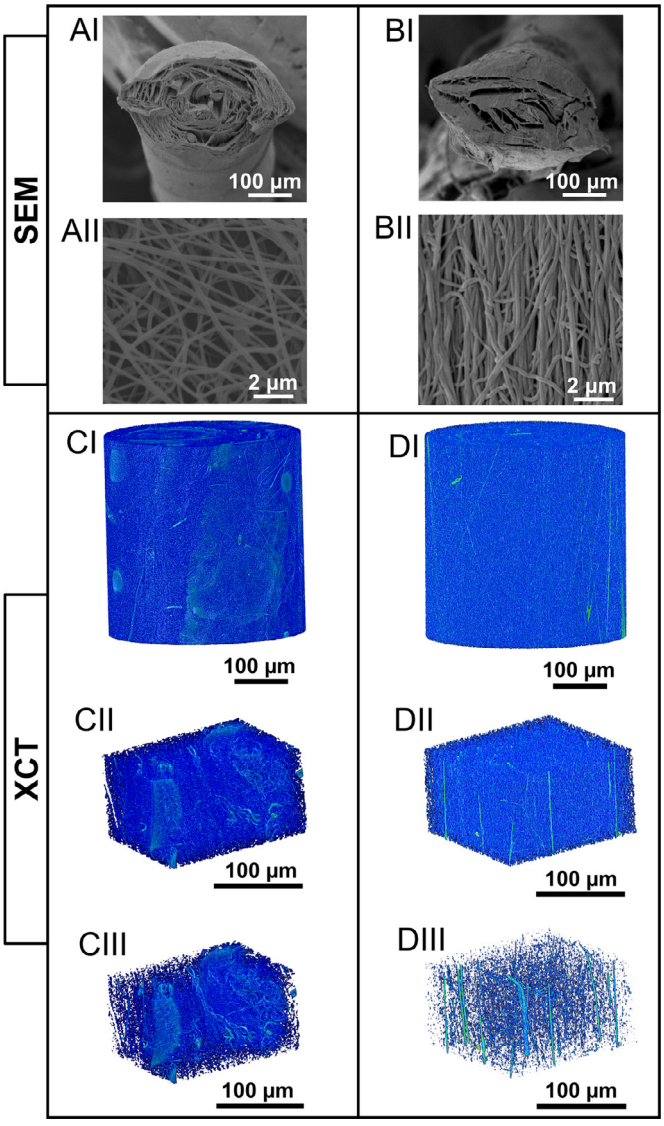

Fig. 3. Imaging of the random and of the aligned bundles. A) SEM images of a random nanofiber bundle. B) SEM images of an aligned nanofiber bundle. The sections of the bundles (magnification = 100x) are visible in part I; the surface of the bundle (magnification = 8000x) are visible in part II. C) XCT images of a random nanofiber bundle; D) XCT images of an aligned nanofiber bundle (0.4 micrometers of voxel size). The sections of the bundles are visible in part I; an internal crop showing the alignment of the nanofibers inside the bundle is reported in part II; tuning the thresholding the most internal nanofibers become visible in part III.

3. Results

3.1. Comparison between random and aligned bundles

The electrospun bundles of random and aligned Nylon 6,6 nanofibers were compared. The random bundles had a cross-sectional diameter of 0.52 ± 0.05 mm, and the aligned bundles of 0.52 ± 0.06 mm. The volume fraction (v) for the random bundles was 0.21 ± 0.03 and 0.30 ± 0.04 for the aligned bundles.

3.1.1. Morphological investigation of the bundles

The SEM investigation showed that the nanofibers of both the random bundles and the aligned bundles were homogeneous, smooth, continuous, and with no defects such as beads (Fig. 3). The nanofibers had consistent mean cross-sectional diameter of 0.23 ± 0.02 micrometers. The different orientation of the nanofibers in the random and in the aligned bundles was clearly visible.

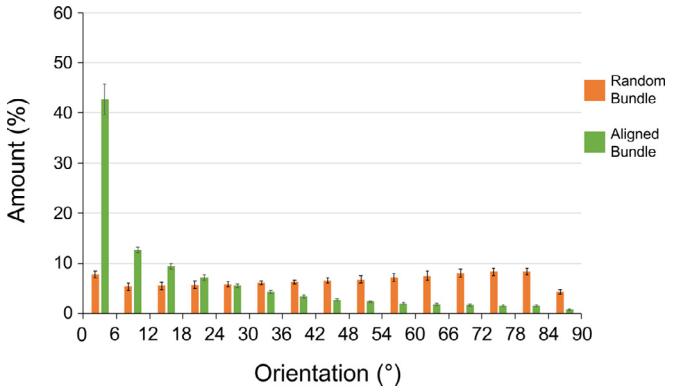

Fig. 4. Directionality of the nanofibers in the random and in the aligned bundles. The directionality histograms show the distribution of the nanofibers in the different directions for the two types of bundles. An angle of 0° means that the nanofibers were aligned with the axis of the bundle, an angle of 90° means that the nanofibers were perpendicular to the bundle.

The XCT investigation of the random bundles showed that nanofibers were randomly arranged both on the surface and inside the bundle (Fig. 3). Few wrapping defects were noted in the internal body of random bundles (Fig. 3).

3.1.2. Directionality of the nanofibers

The Directionality analysis confirmed the different preferential orientation of the nanofibers in the aligned bundles as opposed to the random ones (Fig. 4). The random bundles showed a dispersion of the orientation of the nanofibers so that about 7% of nanofibers fell in each bin. The aligned bundles had a predominant peak in the range of 0°–6° from the bundle axis (42.7% ± 3.1% of the total), and a Gaussian-like distribution. A small amount of nanofibers of 0.78% ± 0.15% was perpendicular to the bundle (84°–90°).

3.1.3. Mechanical properties of the bundles

The load-strain curves revealed a more deformable behavior for the random bundles and a stiffer behavior for the aligned bundles (Fig. 5). Both types of bundles showed a nonlinear toe region up to 1–4% strain (Fig. 5). The random bundles had a failure force of $F_F = 3.27 \pm 0.61$ N, and were weaker than the aligned ones ($F_F = 14.3 \pm 2.7$ N).

After the toe region, the random bundles showed a short elastic region up to an apparent yield stress of $\sigma_Y = 3.27 \pm 0.90$ MPa and a final ductile region up to an apparent failure stress of $\sigma_F = 15.6 \pm 2.8$ MPa (Fig. 5). The aligned bundles also showed higher apparent failure stress ($\sigma_F = 68.7 \pm 15.0$ MPa) compared to the random bundles (Fig. 5). For both of the bundle types, the net mechanical properties were 3–5 times higher than the apparent ones (Table 1).

3.2. Properties of the hierarchical assemblies

The ring-shaped bundles and the hierarchical assemblies made of such bundles were compared. The bundles used for the assemblies were homogeneous, and had a cross-sectional diameter of 0.47 ± 0.04 mm. Three 2nd-level hierarchical assemblies were prepared, each with 24 ring-shaped bundles. The 2nd-level assemblies had a final cross-sectional diameter of 4.3 ± 0.57 mm, and a length of 220 mm (Fig. 6). The bundles inside the assemblies were tightly grouped together and covered with a homogeneous nanofibrous sheath (Fig. 6). The volume fraction (v) for the single bundles was $v = 0.33 \pm 0.02$. The 2nd-level hierarchical assemblies had a lower volume fraction $v = 0.22 \pm 0.05$, due to the free-volume between the single bundles.

The 3rd-level hierarchical assembly had a cross-sectional diameter of 4.6 ± 0.17 mm with a length of 220 mm. Observing the 3rd-level hierarchical assembly, the original 2nd-level hierarchical assemblies were still distinguishable; they were tightly compacted inside the external nanofibrous sheath (Fig. 6). The volume fraction of the 3rd-level hierarchical assembly was $v = 0.175$.

3.2.1. Morphology of the hierarchical assemblies

The SEM investigation showed that the nanofibers in the hierarchical assemblies were homogeneous, smooth, continuous, and with no defects such as beads (Fig. 7). The nanofibers of the electrospun sheaths had consistent mean cross-sectional diameter of 0.23 ± 0.03 micrometers. The bundles were tightly grouped inside the nanofibrous sheaths (Fig. 7).

The XCT investigation on the 2nd-level hierarchical assemblies revealed that the sheath was homogeneous across the surface of the hierarchical assembly, with the presence of some circular defects. In the internal volume of the 2nd-level hierarchical assemblies, the bundles were axially aligned (Fig. 7). The XCT reconstructions of the 3rd-level hierarchical assembly showed that: (i) the nanofibrous sheaths were homogeneous, both the external and the internal with the presence of a few circular defects (Fig. 7) and (ii) the 2nd-level hierarchical assemblies forming the 3rd-level assembly were axially aligned, as well as the single bundles they were made of (Fig. 7).

3.2.2. Alignment of nanofibers of the sheaths and of the internal bundles

The Directionality investigation showed that the nanofibers of the sheaths for the hierarchical assemblies had a slight preferential circumferential orientation (Fig. 8): more than 45% of the nanofibers fell in the range of 66°–90° for the 2nd-level hierarchical assembly; more than 48% of the nanofibers fell in the range of 66°–90° for the 3rd-level assembly.

The preferential axial of alignment of the bundles and the nanofibers inside the bundles was confirmed by the XCT-based Directionality investigation (Fig. 8). All the specimens had a predominant peak in the range of 0°–6° and a Gaussian-like dispersion. The 2nd-level hierarchical assembly showed strong axial alignment, with 52.0% ± 5.1% in the range 0°–6° Similarly, the 3rd-level hierarchical assembly had a strong axial alignment (47.3% ± 5.7% of the nanofibers were peak in the range of 0°–6° from the axis).

3.2.3. Comparison of the mechanical properties of the single bundles and of the hierarchical assembly

The typical load-strain curves of the single ring-shaped bundles and 2nd-level hierarchical assembly confirmed a brittle behavior with a nonlinear toe region up to 1 – 4% of strain (Fig. 9). The single ring-shaped bundles showed a failure force of $F_F = 21.8 \pm 1.7$ N (mean and SD of ten specimens) and the 2nd-level hierarchical assemblies of $F_F = 330 \pm 11.0$ N (mean and SD of three specimens) (Fig. 9).

The bundles had values of apparent failure stress $\sigma_F = 63.4 \pm 10.9$ MPa ($\varepsilon_F = 9.29 \pm 1.02\%$) and the hierarchical assemblies of $\sigma_F = 22.9 \pm 5.0$ MPa ($\varepsilon_F = 8.58 \pm 0.20\%$) respectively (Fig 9). The modulus of elasticity of the single bundles was $E = 877 \pm 83.1$ MPa and for the hierarchical assembly $E = 343 \pm 87.0$ MPa (Fig. 9).

The unit work to failure for the bundles was $L_F = 0.25 \pm 0.08$ J/mm^3 and $L_F = 0.08 \pm 0.02$ J/mm^3 for the 2nd-level hierarchical assemblies (Fig. 9).

The net mechanical properties (computed considering the volume fraction v) were 4–6 times higher than apparent ones (Table. 1).

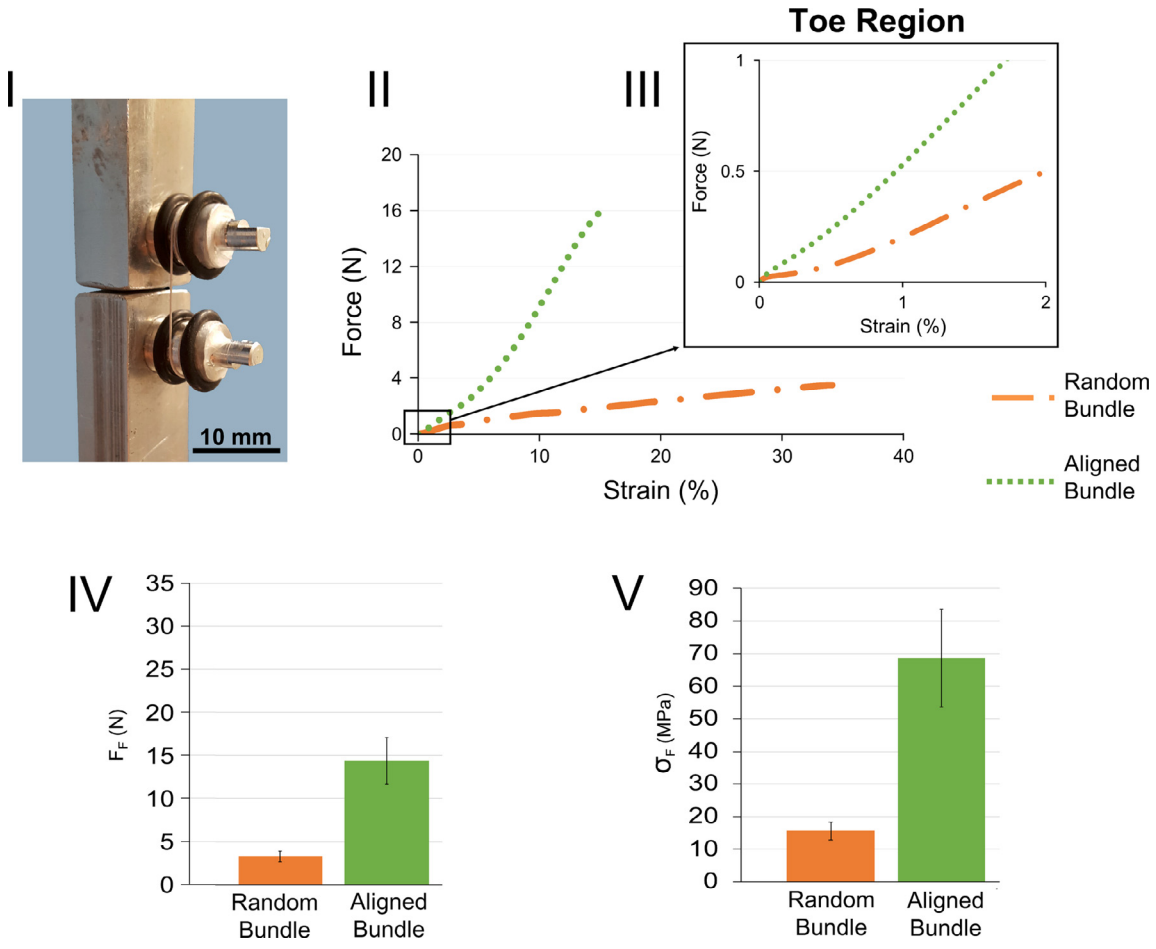

Fig. 5. Mechanical characterization of the bundles of random nanofiber bundles and of aligned nanofibers. I) Tensile test setup with custom-made capstan grips. II) typical load-strain curves of the random bundles and the aligned bundles; III) zoom-in of the nonlinear toe region. Comparison between the mechanical properties of the random and of the aligned bundles: IV) failure force (F_F); V) apparent failure stress (σ_F). The corresponding net mechanical properties are reported in Table 1.

Table 1
Net mechanical properties of the bundles and the 2nd-level hierarchical assemblies obtained from the apparent ones, considering the fraction of volume (v) actually taken by the nanofibers.

	Yield stress (MPa)	Failure stress (MPa)	Modulus of Elasticity (MPa)	Unit work to failure (J/mm^3)
Random Bundle	15.6 ± 3.12	75.5 ± 13.1	–	–
Aligned Bundle	–	235 ± 28.6	–	–
Ring-shaped Bundle	–	389 ± 65.3*	5390 ± 421.1	1.56 ± 0.484
2nd-level Hierarchical Assembly	–	106 ± 4.04*	1589 ± 41.20	0.372 ± 0.0200

*Note**: a slightly lower failure stress was found for the aligned bundles compared to the ring-shaped ones, in relation to the different gripping system (the gripping system used in the first case induced a higher stress concentration than with the ring-shaped bundles).

4. Discussion

The aim of the present study was to develop an innovative morphologically bioinspired electrospun nanofibrous assembly, by using non-resorbable Nylon 6,6, to replicate the hierarchical structure and the mechanical properties of a whole tendon or ligament. Nylon 6,6 was selected for its wide range of clinical applications, such as for suture wires and implantable non-resorbable devices [9].

In order to replicate every single hierarchical level of aggregation of the collagen fibrils inside the tendon and ligament tissue [3,4,14] (Fig. 6), different electrospun bundles were produced.

Firstly, random and aligned nanofiber bundles were obtained by means electrospinning Nylon 6,6 on a drum collector, rotating at different speed. In both cases, the nanofibers had the same diameter of the collagen fibrils [3,4,14] observed within tendons and ligaments. The random bundles were not satisfactory, because they had a morphology and an arrangement of the nanofibers, assessed with SEM and XCT imaging (Fig. 3), far from the tendon and ligament fascicles [36]. Furthermore, their mechanical properties were lower than the human tendon and ligament fascicle [14,37] (Fig. 5). For all these reasons the random bundles were discarded as candidates. The aligned bundles were selected as best fascicle-inspired candidates. Firstly, the SEM and the XCT images (Fig. 3) confirmed that the morphology was similar to the collagen fascicles [3,14,36,38]. The Directionality analysis on the XCT scan of the aligned bundle (Fig. 4) confirmed that the alignment of the Nylon 6,6 nanofibers was similar to that of the tendon and ligament collagen fibrils [39]. Finally, the apparent modulus of elasticity of our Nylon 6,6 aligned bundles (878 ± 83 MPa) was in the same range of the human tendon and ligament fascicles (between 63.5 and 317 MPa [14,37]). The apparent failure stress of the Nylon 6,6 aligned bundles (63.5 ± 11.0 MPa) was superior to the human

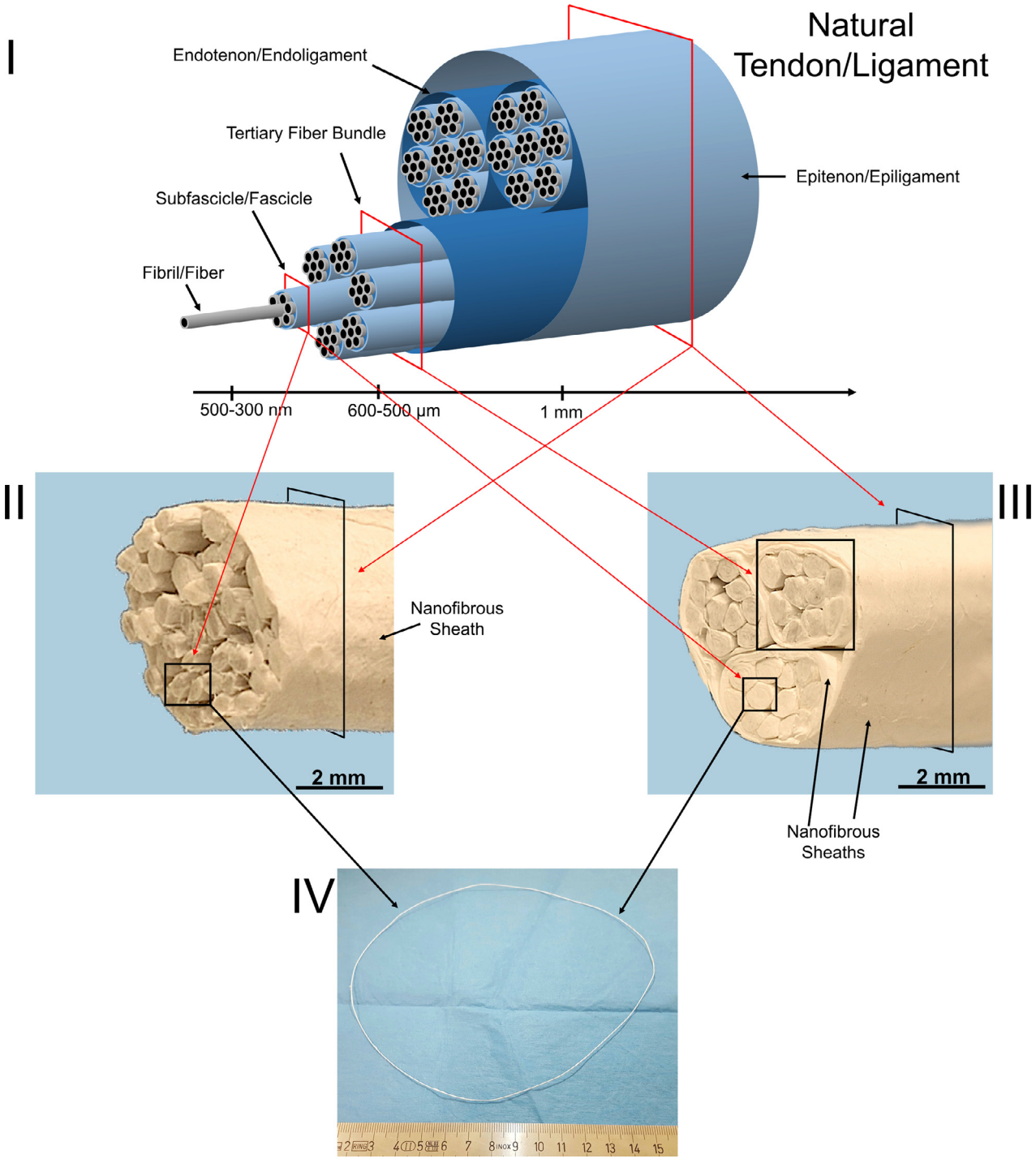

Fig. 6. Comparison between a natural tendon or ligament and the electrospun hierarchical assemblies. I) Hierarchical structure of a tendon or ligament [4]. II) Image of the cross-section of a 2nd-level hierarchical assembly. III) Image of the cross-section of a 3rd-level hierarchical assembly. IV) Image of a ring-shaped bundle used to build the hierarchical assemblies.

tendon and ligament fascicles (between 6.8 and 28.1 MPa [14,37]) (Fig. 5). These findings are consistent with previous studies on electrospun bundles [25,27,40,41].

Subsequently, in order to reproduce the whole structure of a tendon or ligament [3,4,14], several ring-shaped bundles were grouped together, obtaining the 2nd-level hierarchical assembly (Fig. 6). To do this, a dedicated procedure to electrospin sheath was developed (Fig. 1) in order to mimic the morphology of the epitenon/epiligament membranes of tendons and ligaments [3,4,14]. The Directionality analysis on XCT scans confirmed a pronounced axial alignment of the nanofibers inside the 2nd-level assembly, and a slight circumferential alignment of the nanofibers in the outer sheath. Compared to previous similar processes [42–46], our method allowed a finer tuning of the level of compaction of the bundles. In fact, the degree of circumferential orientation can be controlled through the electrospinning procedure by matching the process parameters (i.e. static/rotational time and the rotational speed of the device) during the production of the

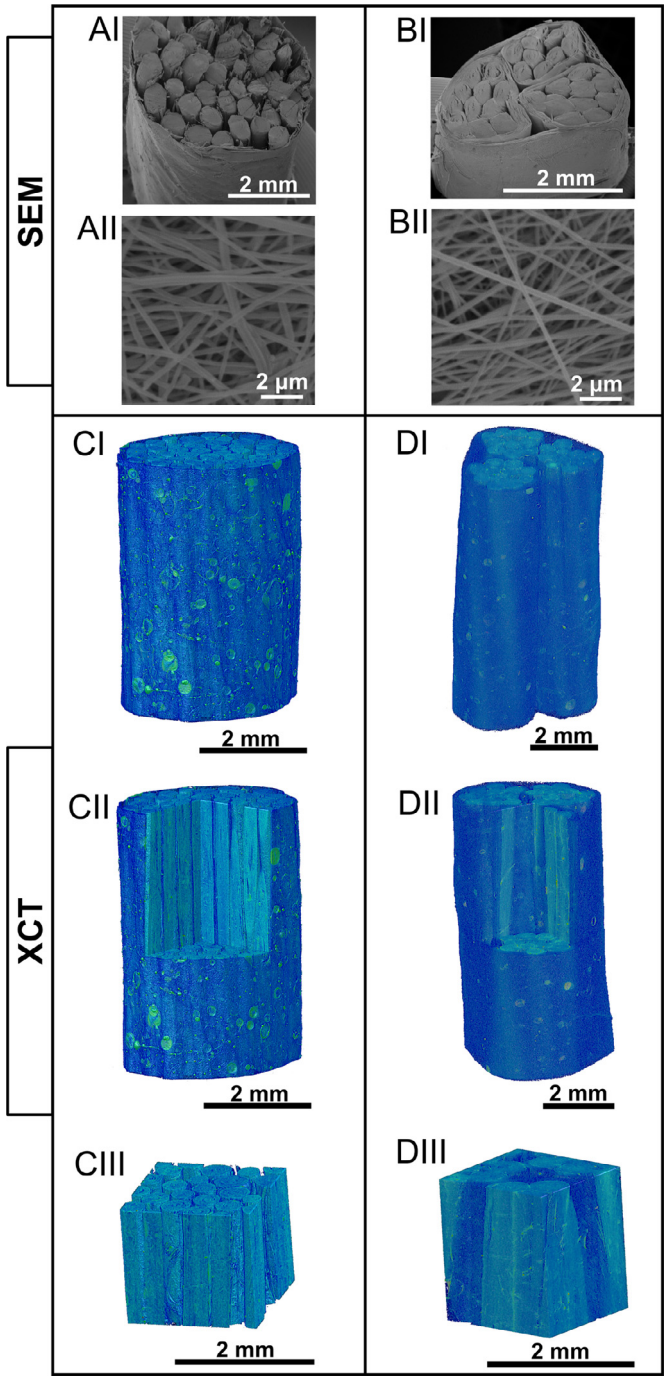

Fig. 7. Imaging of the of the 2nd-level and 3rd-level hierarchical assemblies. A) SEM images of a 2nd-level hierarchical assembly. B) SEM images of a 3rd-level hierarchical assembly. The sections of the hierarchical assemblies (magnification = 25x) are visible in part I; the nanofibers on the surface of the electrospun sheaths (magnification = 8000x) are visible in part II. C) XCT images of a 2nd-level hierarchical assembly (5.27 micrometers voxel size). D) XCT images of a 3rd-level hierarchical assembly (5.27 micrometers voxel size). An external section showing the external electrospun sheath is visible in part I; an external crop showing the internal axially aligned bundles is reported in part II; an internal crop showing the most internal axially aligned bundles are visible in part III.

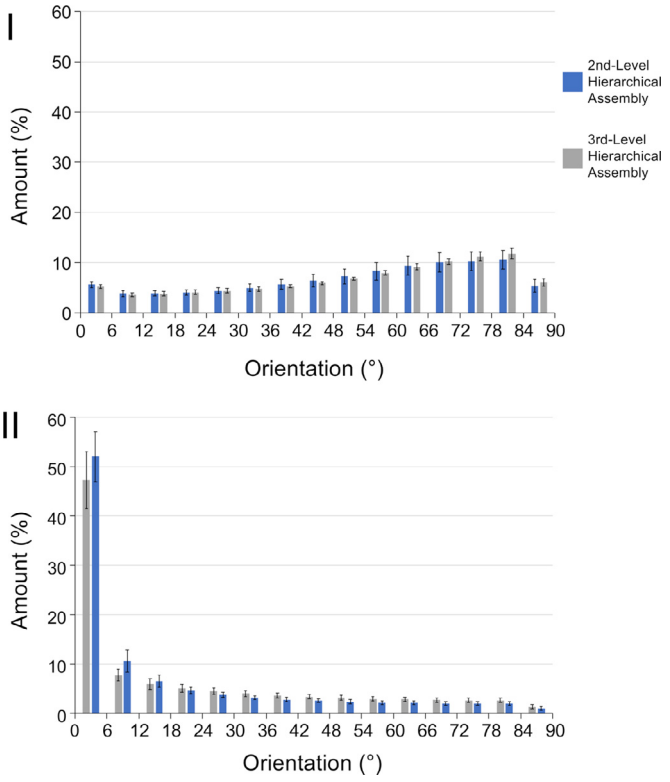

Fig. 8. Comparison between the alignment of the nanofibers in the outer sheaths (I) and inside the assemblies (II) for the 2nd-level and the 3rd-level hierarchical assemblies. An angle of 0° means that the nanofibers were aligned with the axis of the bundle, 90° means that the nanofibers were perpendicular to the bundle.

sheaths (Fig. 8). Thus, it was also possible to adjust the final cross-section of the assemblies themselves, improving their overall mechanical properties (Fig. 9).

As this procedure was particularly flexible, we were able to produce 3rd-level hierarchical assemblies by grouping a number of 2nd-level hierarchical assemblies (Fig. 6). The 3rd-level assemblies incorporate sheaths that mimicked the tendon and ligament endotenon/endoligament membranes [3,4,14]. The Directionality analysis confirmed a pronounced axial alignment of the nanofibers inside the 3rd-level assembly. The slightly lower values of alignment for the 3rd-level assembly compared to the 2nd-level assemblies were caused by the higher percentage of nanofibers in the different sheaths forming the 3rd-level assembly. These hierarchical assemblies showed and unprecedented morphology, biomimicking every single collagen structure that compose a whole natural tendon or ligament [3,4,14].

Both the ring-shaped bundles and the 2nd-level hierarchical assemblies showed a nonlinear toe region up to 1–4% strain, similar to the behavior of the natural fascicles, tendons and ligaments (i.e. 1.5–4%) [5,14,37]. After the toe region, both the bundles and the 2nd-level hierarchical assemblies exhibited a linear elastic behavior, up to 9% strain, before failing (again, similar to the behavior of the natural tendons and ligaments) (Fig. 9). The single bundles had a modulus of elasticity higher than the fascicles of tendons and ligaments [5,14,37]. The hierarchical assembly had a similar modulus of elasticity to natural tendons and ligaments (range: 20–3000 MPa [5,14]). The maximum strain of the bundles was in the same range of collagen fascicles and of natural tendons and ligaments (range: 9–25% [5,37,47]). The failure strain of the hierarchical assemblies was in the range of the natural tendons and ligaments (range: 8–120 MPa [5,14]). The apparent failure stress of the bundles was $\sigma_F = 63.4 \pm 10.9$ MPa. These values were higher than the fascicles of natural tendons and ligaments (range: 6–40 MPa [5,37,47]). The apparent failure stress for the hierarchical assemblies was $\sigma_F = 22.9 \pm 5.0$ MPa, which is in the same range observed in natural tendons and ligaments (range: 1–116 MPa [5,14]). As expected, the modulus of elasticity and the failure stress of the 2nd-level hierarchical assembly was lower than that of the single bundles. This may be due to the fact that the apparent stress in the

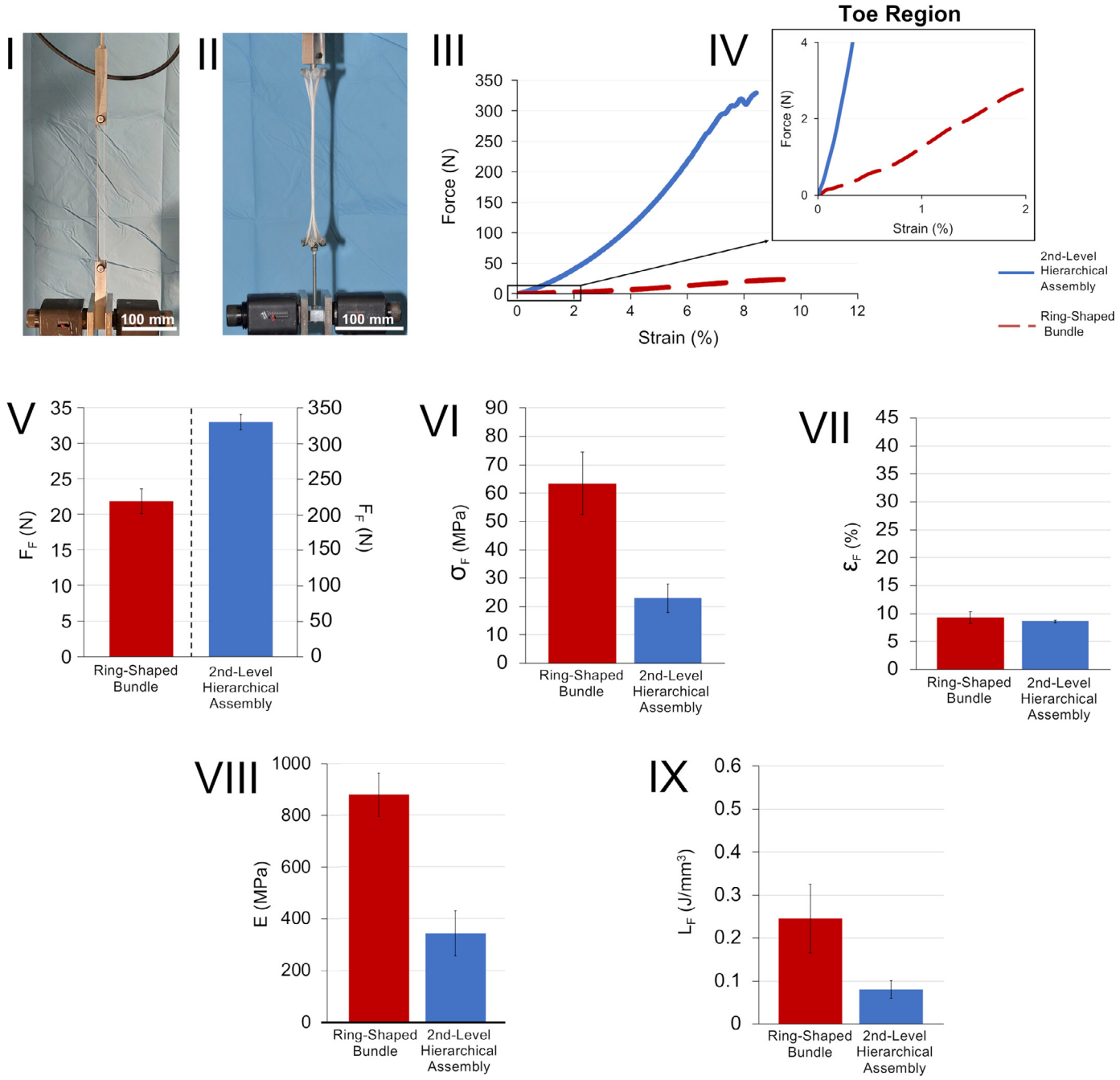

Fig. 9. Mechanical characterization of the ring-shaped bundles and of the 2nd-level hierarchical assembly. I) tensile testing of the ring-shaped bundles using custom-made capstan grips; II) tensile testing of the 2nd-level hierarchical assembly using the 6-arms capstan grips. III) typical load-strain curves of the ring aligned nanofiber bundles and of the 2nd-level hierarchical assemblies; IV) zoom-in the nonlinear toe regions. Comparison between the mechanical properties of the bundles and the 2nd-level hierarchical assemblies: V) failure force (F_F); VI) apparent failure stress (σ_F); VII) failure strain (ε_F); VIII) apparent modulus of elasticity (E); IX) apparent unit work to failure (L_F). The corresponding net mechanical properties are reported in Table 1.

hierarchical assembly is calculated over the total cross-sectional area (which includes the actual cross-section of the bundles, but also some unavoidable empty space). Similarly, the values of net stress (i.e. computed considering the volume fraction actually filled by nanofibers) were significantly higher (4–6 times) than the apparent ones.

Altogether, these properties can grant excellent mechanical performance, and a biomimetic behavior of the hierarchical assembly. Considering that the Nylon 6,6 is an inert material, the possible applications in reconstructive surgery could include replacement of injured tendons or ligaments for the elderly patients (i.e. age greater than 60 years). In fact, due to the low metabolic activity in the elderly, regenerative medicine (i.e. resorbable scaffolds) is not recommended.

Most of the previous electrospun scaffolds reported for tendon and ligament replacements consist of braided, twisted or knitted fibers [46,48–52] which do not replicate the morphology of natural tissues. Compared to previous literature results, the method herein proposed to produce electrospun sheaths confers a better compaction of the single bundles in the multiscale hierarchical scaffold [46,48–52]; thus, providing optimal compromise between morphology and mechanical properties.

Moreover, such high biofidelic hierarchical assemblies will also be suitable as artificial tendons or ligaments for *in vitro* biomechanical validations tests or surgical training. In fact, to the best of our knowledge, there are no specific devices available on the market for such applications. The previous attempts in this field were absolutely trivial and not biomimetic [53–55].

A limitation of this study should be mentioned: some droplets were created during deposition of the electrospun sheaths (Fig. 7). Such defects might have reduced the ability of the sheath to tightly bind the bundles together which might have reduced the improvement in mechanical properties deriving from the compaction of the bundles. In the future, these defects could be avoided by optimizing the flow rate of the Nylon 6,6 solution, possibly further improving the mechanical strength of the assemblies.

The XCT investigation was extremely challenging because of the small diameter of the electrospun nanofibers, and of the low attenuation of the polymer [31,41,51,52,56,57]. Videos of the XCT scans of a single bundle of aligned nanofibers and of 2nd-level hierarchical assembly are available in the Supplementary Materials through ScienceDirect. Additional images and videos of the XCT scans are available through Figshare (single aligned bundle: https://doi.org/10.6084/m9.figshare.7636580.v4; 2nd-level hierarchical assembly: https://doi.org/10.6084/m9.figshare.7636592.v3; 3rd-level hierarchical assembly: https://doi.org/10.6084/m9.figshare.7636595.v3).

In conclusion this work showed an innovative electrospinning production process to design and build nanofibrous Nylon 6,6 hierarchical assemblies, suitable as future implantable devices, able to mimic the multiscale morphology and the biomechanical properties of tendons and ligaments.

Acknowledgments

The Italian Ministry of University and Research (MIUR) is acknowledged. The mobility of Alberto Sensini was funded by the University of Bologna (Marco Polo grant). The Zeiss Global Centre at the University of Portsmouth is greatly acknowledged for the support in X-ray imaging and data post-processing. The authors gratefully acknowledge the Giuseppe Valli for the valuable suggestions and for 3D-printing the 6-arms capstan grips.

Competing interest

None declared.

Funding

Funding from the Italian Ministry of University and Research (MIUR) is acknowledged. The mobility of Alberto Sensini was funded by the University of Bologna (Marco Polo grant).

Ethical approval

Not required.

Supplementary materials

Supplementary material associated with this article can be found, in the online version, at doi:10.1016/j.medengphy.2019.06.019.

References

[1] Abbah SA, Spanoudes K, O'Brien T, Pandit A, Zeugolis D. Assessment of stem cell carriers for tendon tissue engineering in pre-clinical models. Stem Cell Res Ther 2014;5:1–9. doi:10.1186/scrt426.

[2] Zeugolis DI, Chan JCY, Pandit A. Tendons: engineering of functional tissues. In: Pallua N, Suscheck C, editors. Tissue engineering. From lab to clinic. Tissue engineering. Berlin Heidelberg: Springer; 2011. p. 1–634. doi:10.1007/978-3-642-02824-3.

[3] Kastelic J, Galeski A, Baer E. The multicomposite structure of tendon. Connect Tissue Res 1978;6:11–23. doi:10.3109/03008207809152283.

[4] Kannus P. Structure of the tendon connective tissue. Scand J Med Sci Sport 2000;10:312–20. doi:10.1034/j.1600-0838.2000.010006312.x.

[5] Goh KL, Listrat A, Béchet D. Hierarchical mechanics of connective tissues: integrating insights from nano to macroscopic studies. J Biomed Nanotechnol 2014;10:2464–507. doi:10.1166/jbn.2014.1960.

[6] McCarthy MM, Hannafin JA. The mature athlete: aging tendon and ligament. Sports Health 2014;6:41–8. doi:10.1177/1941738113485691.

[7] Woo SLY, Hollis JM, Adams DJ, Lyon RM, Takai S. Tensile properties of the human femur-anterior cruciate ligament-tibia complex: the effects of specimen age and orientation. Am J Sports Med 1991;19:217–25. doi:10.1177/036354659101900303.

[8] Chen J, Xu J, Wang A, Zheng M. Scaffolds for tendon and ligament repair: review of the efficacy of commercial products. Expert Rev Med Devices 2014;6:61–73. doi:10.1586/17434440.6.1.61.

[9] Maitz MF. Applications of synthetic polymers in clinical medicine. Biosurface Biotribology 2015;1:161–76. doi:10.1016/j.bsbt.2015.08.002.

[10] Capperauld I. Suture materials: a review. Clin Mater 1989;4:3–12. doi:10.1016/0267-6605(89)90021-8.

[11] Boileau P, Brassart N, Watkinson DJ, Carles M, Hatzidakis AM, Krishnan SG. Arthroscopic repair of full-thickness tears of the supraspinatus: does the tendon really heal? J Bone Jt Surg - Ser A 2005;87:1229–40. doi:10.2106/JBJS.D.02035.

[12] Longo UG, Lamberti A, Maffulli N, Denaro V. Tendon augmentation grafts: a systematic review. Br Med Bull 2010;94:165–88. doi:10.1093/bmb/ldp051.

[13] Jackson DW, Heinrich JT, Simon TM. Biologic and synthetic implants to replace the anterior cruciate ligament. Arthrosc J Arthrosc Relat Surg 1994;10:442–52. doi:10.1016/S0749-8063(05)80197-5.

[14] Murphy W, Black J, Hastings G. Handbook of biomaterial properties. Second. Springer; 2016. doi:10.1007/978-1-4939-3305-1.

[15] Batty LM, Norsworthy CJ, Lash NJ, Wasiak J, Richmond AK, Feller JA. Synthetic devices for reconstructive surgery of the cruciate ligaments: a systematic review. Arthrosc - J Arthrosc Relat Surg 2015;31:957–68. doi:10.1016/j.arthro.2014.11.032.

[16] Brunet P, Charrois O, Degeorges R, Boisrenoult P, Beaufils P. Reconstruction of acute posterior cruciate ligament tears using a synthetic ligament. Rev Chir Orthop Reparatrice Appar Mot 2005;91:34–43 doi:MDOI-RCO-02-2005-91-1-0035-1040-101019-200510479 [pii].

[17] Engstrom B., Wredmark T., Westblad P. Patellar tendon or leeds-keio graft in the surgical treatment of anterior cruciate ligament ruptures. Intermed Results. Clin Orthop Relat Res 1993:190–7.

[18] Ochi M, Yamanaka T, Sumen Y, Ikuta Y. Arthroscopic and histologic evaluation of anterior cruciate ligaments reconstructed with the leeds-keio ligament. Arthrosc J Arthrosc Relat Surg 1993;9:387–93. doi:10.1016/S0749-8063(05)80312-3.

[19] Rading J, Peterson L. Clinical experience with the leeds-keio artificial ligament in anterior cruciate ligament Reconstruction: a prospective two-year Follow-up study. Am J Sports Med 1995;23:316–19. doi:10.1177/036354659502300311.

[20] Murray AW, Macnicol MF. 10–16 year results of leeds-keio anterior cruciate ligament reconstruction. Knee 2004;11:9–14. doi:10.1016/S0968-0160(03)00076-0.

[21] Hirooka A, Yoneda M, Wakaitani S, Isaka Y, Hayashida K, Fukushima S, et al. Augmentation with a gore-tex patch for repair of large rotator cuff tears that cannot be sutured. J Orthop Sci 2002;7:451–6. doi:10.1007/s007760200078.

[22] Kollender Y, Bender B, Weinbroum AA, Nirkin A, Meller I, Bickels J. Secondary reconstruction of the extensor mechanism using part of the quadriceps tendon, patellar retinaculum, and gore-tex strips after proximal tibial resection. J Arthroplasty 2004;19:354–60. doi:10.1016/j.arth.2003.11.004.

[23] Muren O, Dahlstedt L, Brosjö E, Dahlborn M, Dalén N. Gross osteolytic tibia tunnel widening with the use of gore-tex anterior cruciate ligament prosthesis: a radiological, arthrometric and clinical evaluation of 17 patients 13-15 years after surgery. Acta Orthop 2005;76:270–4. doi:10.1080/00016470510030689.

[24] Miller MD, Peters CL, Allen B. Early aseptic loosening of a total knee arthroplasty due to gore-tex particle-induced osteolysis. J Arthroplasty 2006;21:765–70. doi:10.1016/j.arth.2005.07.021.

[25] O'Connor RA, McGuinness GB. Electrospun nanofibre bundles and yarns for tissue engineering applications: a review. Proc Inst Mech Eng Part H J Eng Med 2016;230:987–98. doi:10.1177/0954411916656664.

[26] Brennan DA, Conte AA, Kanski G, Turkula S, Hu X, Kleiner MT, et al. Mechanical considerations for electrospun nanofibers in tendon and ligament repair. Adv Healthc Mater 2018;1701277:1–31. doi:10.1002/adhm.201701277.

[27] Sensini A, Cristofolini L. Biofabrication of electrospun scaffolds for the regeneration of tendons and ligaments. Materials (Basel) 2018;11:1963. doi:10.3390/ma11101963.

[28] Liu Z. Scale space approach to directional analysis of images. Appl Opt 1991;30:1369–73. doi:10.1364/AO.30.001369.

[29] Schindelin J, Arganda-Carreras I, Frise E, Kaynig V, Longair M, Pietzsch T, et al. Fiji: an open-source platform for biological-image analysis. Nat Methods 2012;9:676–82. doi:10.1038/nmeth.2019.

[30] Schneider CA, Rasband WS, Eliceiri KW. NIH image to ImageJ: 25 years of image analysis. Nat Methods 2012;9:671–5. doi:10.1038/nmeth.2089.
[31] Sensini A, Cristofolini L, Focarete ML, Belcari J, Zucchelli A, Kao A, et al. High-resolution x-ray tomographic morphological characterisation of electrospun nanofibrous bundles for tendon and ligament regeneration and replacement. J Microsc 2018;272:196–206. doi:10.1111/jmi.12720.
[32] Butler DL. Anterior cruciate ligament: its normal response and replacement. J Orthop Res 1989;7:910–21. doi:10.1002/jor.1100070618.
[33] Lewis G, Shaw KM. Tensile properties of human tendo Achillis: effect of donor age and strain rate. J Foot Ankle Surg 1997;36:435–45. doi:10.1016/S1067-2516(97)80096-8.
[34] Wren TA, Yerby SA, Beaupré GS, Carter DR. Mechanical properties of the human achilles tendon. Clin Biomech 2001;16:245–51. doi:10.1016/S0268-0033(00)00089-9.
[35] Lee M, Hyman W. Modeling of failure mode in knee ligaments depending on the strain rate. BMC Musculoskelet Disord 2002;3:1–8. doi:10.1186/1471-2474-3-3.
[36] Moshiri A, Oryan A. Tendon and ligament tissue engineering, healing and regenerative medicine. J Sports Med Doping Stud 2013;3:1–18. doi:10.4172/2161-0673.1000126.
[37] Hanson P, Aagaard P, Magnusson SP. Biomechanical properties of isolated fascicles of the iliopsoas and achilles tendons in African American and Caucasian men. Ann Anat 2012;194:457–60. doi:10.1016/j.aanat.2012.03.007.
[38] Kannus P, Paavola M, Józsa L. Aging and degeneration of tendons. In: Maffulli N, Renström P WB L, editors. Tendon injury. London: Springer; 2005. p. 25–31. doi:10.1007/1-84628-050-8_4.
[39] Provenzano PP, Vanderby R. Collagen fibril morphology and organization: implications for force transmission in ligament and tendon. Matrix Biol 2006;25:71–84. doi:10.1016/j.matbio.2005.09.005.
[40] Sensini A, Gualandi C, Cristofolini L, Tozzi G, Dicarlo M, Teti G, et al. Biofabrication of bundles of poly(lactic acid)-collagen blends mimicking the fascicles of the human achille tendon. Biofabrication 2017;9. doi:10.1088/1758-5090/aa6204.
[41] Sensini A, Gualandi C, Zucchelli A, Boyle L, Kao AP, Reilly GC, et al. Tendon fascicle-inspired nanofibrous scaffold of polylactic acid/Collagen with enhanced 3D-Structure and biomechanical properties. Sci Rep 2018;8:1–15. doi:10.1038/s41598-018-35536-8.
[42] Zhou FL, Gong R-H, Porat I. Nano-coated hybrid yarns using electrospinning. Surf Coatings Technol 2010;204:3459–63. doi:10.1016/j.surfcoat.2010.04.021.
[43] Kohlman L.W., Roberts G.D. Method for coating tow with an electrospun nanofiber. US8932683B1, 2015. doi:10.1016/j.(73).
[44] Naghashzargar E, Farè S, Catto V, Bertoldi S, Semnani D, Karbasi S, et al. Nano/micro hybrid scaffold of PCL or P3HB nanofibers combined with silk fibroin for tendon and ligament tissue engineering. J Appl Biomater Funct Mater 2015;13:e156–68. doi:10.5301/jabfm.5000216.
[45] Li D, Pan X, Sun B, Wu T, Chen W, Huang C, et al. Nerve conduits constructed by electrospun P(LLA-CL) nanofibers and PLLA nanofiber yarns. J Mater Chem B 2015;3:8823–31. doi:10.1039/C5TB01402F.
[46] Banik BL, Lewis GS, Brown JL. Multiscale Poly-(ϵ-caprolactone) scaffold mimicking Non-linearity in tendon tissue mechanics. Regen Eng Transl Med 2016;2:1–9. doi:10.1007/s40883-016-0008-5.
[47] Butler DL, Kay MD, Stouffer DC. Fascicle-Bone units from human patellar tendon and knee ligaments. J Biomech 1986;19:425–32. doi:10.1016/0021-9290(86)90019-9.
[48] Xu Y, Dong S, Zhou Q, Mo X, Song L, Hou T, et al. The effect of mechanical stimulation on the maturation of TDSCs-poly(L-lactide-co-e-caprolactone)/collagen scaffold constructs for tendon tissue engineering. Biomaterials 2014;35:2760–72. doi:10.1016/j.biomaterials.2013.12.042.
[49] Bosworth LA. Travelling along the clinical Roadmap: developing electrospun scaffolds for tendon repair. In: Proceedings of the conference paper science, 2014; 2014. p. 1–6. doi:10.1155/2014/304974.
[50] Mouthuy P-A, Zargar N, Hakimi O, Lostis E, Carr A. Fabrication of continuous electrospun filaments with potential for use as medical fibres. Biofabrication 2015;7:25006. doi:10.1088/1758-5090/7/2/025006.
[51] Laranjeira M, Domingues RMA, Costa-Almeida R, Reis RL, Gomes ME. 3D Mimicry of native-tissue-fiber architecture guides tendon-derived cells and adipose stem cells into artificial tendon constructs. Small 2017;13:1–13. doi:10.1002/smll.201700689.
[52] Abhari RE, Mouthuy PA, Vernet A, Schneider JE, Brown CP, Carr AJ. Using an industrial braiding machine to upscale the production and modulate the design of electrospun medical yarns. Polym Test 2018;69:188–98. doi:10.1016/j.polymertesting.2018.05.014.
[53] Tare M. Dental rolls: a suitable model for practising tendon repair techniques. J Hand Surg Am 2004;29:506–7. doi:10.1016/j.jhsb.2004.05.006.
[54] Ingraham JM, Weber RA, Weber RA. Utilizing a simulated tendon to teach tendon repair technique. Hand 2009;4:150–5. doi:10.1007/s11552-009-9184-9.
[55] Abdulal S, Onyekwelu O. An alternative model for teaching tendon repair and surgical skills in plastic surgery. JPRAS Open 2016;7:12–15. doi:10.1016/j.jpra.2015.11.003.
[56] Bosworth LA, Rathbone SR, Bradley RS, Cartmell SH. Dynamic loading of electrospun yarns guides mesenchymal stem cells towards a tendon lineage. J Mech Behav Biomed Mater 2014;39:175–83. doi:10.1016/j.jmbbm.2014.07.009.
[57] Bradley RS, Robinson IK, Yusuf M. 3D X-Ray nanotomography of cells grown on electrospun scaffolds. Macromol Biosci 2017;17:1–8. doi:10.1002/mabi.201600236.